Steady-state behavior of ring polymers in dilute flowing solutions via Brownian dynamics

J.G. Hernández Cifre[*], R. Pamies, M.C. López Martínez, J. García de la Torre

Departamento de Química Física, Facultad de Química Universidad de Murcia, 30071 Murcia, Spain

Abstract

A bead and spring model is considered for the Brownian dynamics simulation of the behavior of cyclic polymer chains (rings) in a dilute solution under shear or elongational flow. Finite extensibility, excluded volume, and hydrodynamic interaction are taken into account to make the polymer model as realistic as possible. In shear flow, the deformation of the chain and the shear rate viscosity dependence (the flow curve), are studied and characterized. In elongational flow, the coil-stretch phenomenon is described and the relationship between the critical elongational rate and the molecular weight is given. The qualitative behavior obtained for ring polymers is analogous to that of linear polymers.
© 2004 Elsevier Ltd. All rights reserved.

Keywords: Brownian dynamics; Bead-and-spring; Dilute solution

1. Introduction

The study of the behavior of flexible polymer chains in a flowing solution has received an important impulse during the past decades due to the advent of powerful computational techniques that allow for the inclusion of more realistic effects in the polymer models. Most efforts have been devoted to solve conformational and dynamical problems of linear polymer under both shear and extensional flows.

In simple shear it is well known that polymer chains are oriented and deformed, which influences the solution flow properties, thus appearing the characteristic non-Newtonian behavior. On the other hand, under extensional flows, flexible polymer chains experience the so-called coil-stretch transition [1,2], consisting of the abrupt, sudden, increase in polymer property values when the extensional rate exceeds a certain critical value. Previous papers of our group [3,4] are devoted to the study of such systems, and show the importance of the inclusion of effects such a excluded volume (EV) and hydrodynamic interaction (HI) in order to get results comparable to experiments.

Notwithstanding the huge amount of work on flowing polymer solutions, less attention has been paid to polymers with non-linear topology, mainly to the so-called ring polymers. The improvement of experimental techniques that allows for both synthesis and accurate characterization of ring polymers makes the theoretical study of these non-linear structures of great practical interest. Equilibrium properties of flexible cyclic chains have been studied in some extent analytically (see Refs. [5,6] and references therein), experimentally [7–9], and numerically [7,8,10,11]. A review of the recent advances in the topic of cyclic polymers is found in Ref. [12]. In this paper, we show the behavior of such ring polymers under two typical flow situations: simple shear and steady uniaxial elongational flow. For such a study, we make use of the Brownian dynamics simulation technique (BD). We do not show comparison to experimental data. We hope our simulation results will be of interest for the interpretation of the behavior of dilute ring polymer solutions under flow, for which no much experimental work is available.

2. Model and methodology

We consider a dilute solution of ring polymers subjected to both simple shear and steady elongational flows. The

* Corresponding author. Tel.: +34 968 367420; fax: +34 968 364148.
E-mail address: jghc@um.es (J.G. Hernández Cifre).

velocity field of the shear flow is given by

$$v_x = \dot{\gamma}y, \quad v_y = 0, \quad v_z = 0 \tag{1}$$

whereas the elongational velocity field is given by

$$v_x = \dot{\varepsilon}x, \quad v_y = -\frac{1}{2}\dot{\varepsilon}y, \quad v_x = -\frac{1}{2}\dot{\varepsilon}z \tag{2}$$

where $\dot{\gamma}$ and $\dot{\varepsilon}$ are the shear rate and the elongational rate respectively. In shear flow, it is convenient to use a dimensionless form of the shear rate related to the molecular weight of the polymer chain

$$\beta = \frac{M\eta_s[\eta]_0}{N_A k_B T}\dot{\gamma} \tag{3}$$

where M is the molecular weight, η_s is the solvent viscosity, $[\eta]_0$ the zero-shear intrinsic viscosity, N_A the Avogadro number and $k_B T$ the Boltzmann factor.

The polymer molecule is modeled as a cyclic bead-and-spring chain [13] with N beads connected by N FENE (finite extensible non-linear elongational) springs which follow the force law [13]

$$\mathbf{F}^{(s)} = -\frac{H}{1 - (Q/Q_{max})^2}\mathbf{Q} \tag{4}$$

where $\mathbf{Q}$ is the spring vector, Q_{max} the maximum spring length and $H = 3k_B T/b^2$ the spring constant, being b^2 the equilibrium mean squared length of a Hookean spring. For checking purposes some simulations were carried out using Hookean springs which follow the linear law $\mathbf{F}^{(s)} = H\mathbf{Q}$.

Intramolecular, excluded volume interactions to mimic solvent quality are simulated by introducing interaction forces between non-neighboring beads. An adequate choice is the Lennard-Jones (LJ) potential

$$V = 4\varepsilon_{LJ}\left[\left(\frac{\sigma_{LJ}}{r_{ij}}\right)^{12} - \left(\frac{\sigma_{LJ}}{r_{ij}}\right)^6\right] \tag{5}$$

where r_{ij} is the distance between beads i and j and ε_{LJ} and σ_{LJ} are the Lennard-Jones parameters: minimum energy and zero energy distance, respectively. As shown by Freire and co-workers, appropriate LJ parameter values that reproduce correctly the power laws of polymer properties are $\varepsilon_{LJ} = 0.1k_B T$ for good solvents [14] and $\varepsilon_{LJ} = 0.3k_B T$ for theta solvents [15], with $\sigma_{LJ} = 0.8b$ in any case. Therefore, we adopt those values in the present work.

The dynamics of the polymer chain is monitored from trajectories of individual molecules obtained by BD simulation. We employ a predictor–corrector version of the Ermak and McCammon algorithm [16] proposed by Iniesta and García de la Torre [17]. Simulations with and without HI were performed. Fluctuating hydrodynamic interaction between beads is taken into account using the Rotne–Prague–Yamakawa tensor [18,19]. For the bead friction, we use a Stokes coefficient $\zeta = 6\pi\eta_s\sigma$, where the bead radius

$\sigma = 0.257b$, which corresponds to a dimensionless HI parameter $h^* = (\zeta/6\pi\eta_s)\sqrt{H/\pi k_B T} = 0.25$. In this way, five independent polymer trajectories are generated. Steady-state properties are computed by averaging over each trajectory, after discounting the initial part for equilibration purposes. Then, the mean and standard deviation over the five trajectories are taken to characterize the actual property values.

In this work, quantities are given in dimensionless units (indicated with an asterisk as superscript). This is accomplished by dividing length by the equilibrium root-mean-square spring length, b, energy by $k_B T$ and time by $\zeta b^2/K_B T$. In this unit system, the spring constant becomes $H^* = 3$ and the maximum spring length $Q^*_{max} = 10$. This value, used in previous works [4], corresponds to a value of the so-called extensibility parameter about 100, adequate to represent highly flexible polymer chains [20]. The simulation time step is $\Delta t^* = 10^{-4}$, as required by the very steep behavior of the Lennard-Jones potential.

3. Results

3.1. Equilibrium

Before presenting the flow behavior of ring polymers, we briefly show equilibrium results, i.e., in the absence of flow, performed for testing purposes. Thus, we reconsider the calculations carried out by Bernal et al. [10,11] over 10 years ago using the Monte Carlo technique and try to verify their results using a more extensive computation. It is usual to define the ratio between a ring polymer property and its linear counterpart, i.e., that of a linear chain with identical number of beads, N. Thus, $q_{s,0} = \langle s^2\rangle_{r,0}/\langle s^2\rangle_{l,0}$ and $q_{\eta,0} = [\eta]_{r,0}/[\eta]_{l,0}$, where $\langle s^2\rangle$ is the mean squared radius of gyration, $[\eta]$ the intrinsic viscosity, the subscripts r and l stand for ring and linear, respectively and subscript zero refers to the solution at rest (no flow). When no HI and no EV are considered, it is shown that $q_{s,0} = q_{\eta,0} = 1/2$ [6]. Our simulation results agree quite well with this behavior as well as with the previous Monte Carlo simulations performed by Bernal et al. [10,11]. Taking into account HI effects, we get, in the absence of EV, $q_{\eta,0} \sim 0.53$ and $q_{s,0} \sim 0.50$, and for good solvent conditions, $q_{\eta,0} \sim 0.59$ and $q_{s,0} \sim 0.54$. The values of these ratios are independent of N provided N is large enough so that they were obtained averaging their simulation values for various chain lengths N. Nevertheless, those ratios are slightly sensitive to the model used to describe the polymer as shown in previous works [10]. Furthermore, there are difficulties in establishing the conditions under which the solvent quality degree for a ring chain can be compared to that for a linear chain [10,21]. A classical quantity that is free of these inconsistencies is the Flory parameter, Φ. We have determined the value of this constant for ring polymers with HI from our simulations

as

$$\Phi = \frac{[\eta]^* N_A}{(6\langle s^2 \rangle^*)^{3/2}} \qquad (6)$$

The Flory parameter presents a slight variation with the number of beads of the chain. Therefore, we computed Φ for several chain lengths, from $N = 12$ up to $N = 91$, and made the extrapolation to the long chain limit, i.e. $1/\sqrt{N} \to 0$, as illustrated in Fig. 1. Thus, we obtained for theta solvents $\Phi \times 10^{-23} \simeq 3.8$–4.0, depending on the inclusion or not (ideal chain) of LJ potential in the simulation, and $\Phi \times 10^{-23} \simeq 2.8$ in good solvents. These results are in very good agreement with the values from Bernal et al. [10,11].

Finally, we also show that the ring polymer model used in our simulations reproduces the equilibrium power laws relating $\langle s^2 \rangle_{r,0}$ and $[\eta]_{r,0}$ with the molecular weight, i.e. number of beads N. Thus, in Fig. 2 we can observe the N dependency of $\langle s^2 \rangle_{r,0}$ and $[\eta]_{r,0}$ altogether, for both theta and good solvent conditions and with HI. From the slopes of those plots, we obtain that in theta solvent $\langle s^2 \rangle_{r,0} \propto N^{1.006 \pm 0.003}$ and $[\eta]_{r,0} \propto N^{1.626 \pm 0.003}$, and in good solvent $\langle s^2 \rangle_{r,0} \propto N^{1.189 \pm 0.003}$ and $[\eta]_{r,0} \propto N^{1.805 \pm 0.003}$. The exponents of the foregoing scaling relationships, which also holds for linear chains, agree quite well with results in [11] as well as with their theoretical values (e.g. $\langle s^2 \rangle_{r,0}(\text{theta}) \propto N^1$, $[\eta]_{r,0}(\text{theta}) \propto N^{1.5}$, $\langle s^2 \rangle_{r,0}(\text{good}) \propto N^{1.2}$, $[\eta]_{r,0}(\text{good}) \propto N^{1.8}$), except for the intrinsic viscosity at theta conditions, which is slightly higher than the expected value 1.5. Perhaps Lennard-Jones parameters representing theta conditions for ring chains should be reconsidered.

3.2. Shear flow

We study the influence of the shear rate β on both the polymer dimensions, in terms of the parameter δ^2, which gives the relative increase in the mean-square radius of gyration
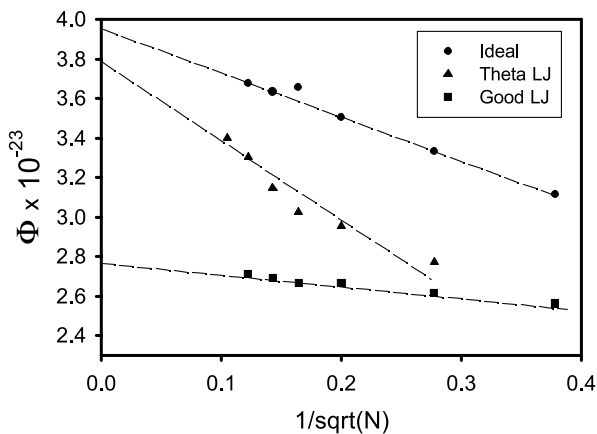

Fig. 1. Dependence of the Flory parameter with the chain length, N, for several solvent conditions and with HI. Extrapolation to $N \to \infty$.
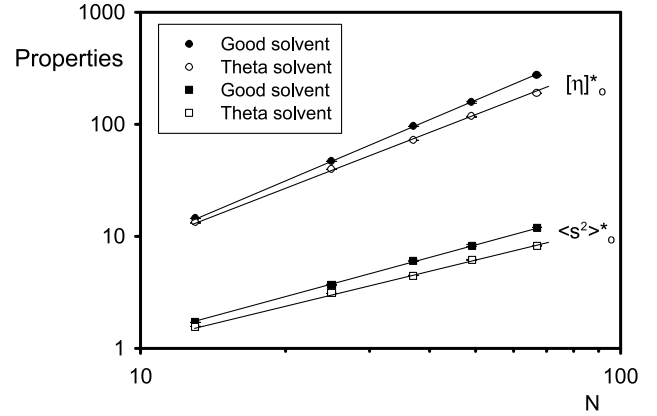

Fig. 2. Variation of $\langle s^2 \rangle_0^*$ and $[\eta]_0^*$ (solution at rest) with the number of beads of the ring, for both theta and good solvent conditions and with HI.

$$\delta^2 = \frac{\langle s^2 \rangle}{\langle s^2 \rangle_0} - 1 \qquad (7)$$

which measures the polymer deformation, and on the intrinsic viscosity

$$[\eta] = -\frac{N_A}{\eta_s n M} \frac{(\tau_{xy})_p}{\dot{\gamma}} \qquad (8)$$

where n is the number concentration of polymer and $(\tau_{xy})_p$ the polymer contribution to the shear stress. For a bead-and-spring macromolecular model, the stress tensor is calculated using the modified Kramers expression [13]

$$\tau_{\alpha,\beta} = \sum_{i=1}^{N} \langle \mathbf{R}_{i,\alpha} \cdot \mathbf{F}_{i,\beta}^{(s)} \rangle \qquad (9)$$

where $\alpha, \beta = x, y, z$, R_i is the position vector of a bead i respect to the center of mass of the chain and $F_i^{(s)}$ is the total spring force on bead i. The brackets $\langle \rangle$ mean conformational average.

Fig. 3(a) shows the evolution of δ^2 with β for various polymer lengths, N, in good solvent conditions ($\varepsilon_{LJ}^* = 0.1$) and with HI. The aspect of those plots are similar to that for linear chains with both FENE and Hookean springs [3]. Thus, at low and moderate shear rates, δ^2 follows a straight line in a log–log plot. Besides, values of δ^2 for different N tend to superimpose, since β makes results molecular weight independent at low shear rates. At high shear rates, however, a downward curvature appears as a consequence of the finite chain extensibility, and asymptotic δ^2 values differ, increasing with the number of beads, N. The influence of the excluded volume effects on δ^2 is shown in Fig. 3(b). The shear rate dependence of the deformation reflects the complex interplay of the effects of hydrodynamic interaction, excluded volume and finite extensibility. These effects have been evaluated for linear chains [22–24]. The dependence can be expressed by a power law,

$$\delta^2 = C\beta^a \qquad (10)$$

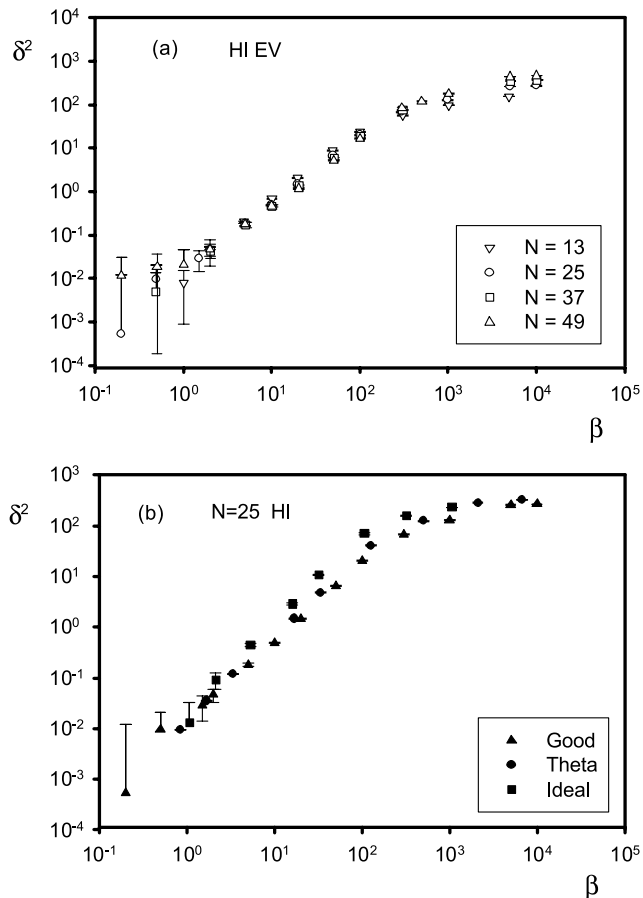For ideal (no EV, infinitely extensible) Gaussian chains with

Fig. 3. (a) Dependence of the ring deformation, δ^2, with the shear rate, β, for chains with several N with HI and good solvent conditions. (b) Dependence of δ^2 with β for a ring with $N=25$, HI and several solvent conditions.

HI, this law holds with an exponent $a=2$—although with different C constants—in the two limits of very low and very high β, but there is an intermediate region in which the HI effects vanish gradually as β increases [23]. Furthermore, when EV effects are introduced, the apparent exponent is variable with shear rate and smaller than 2 [24]. Finally, the introduction of finite extensibility dominates the high shear region.

In the region of intermediate β, our present results for ring polymers can be fitted to Eq. (10) with the values of a that are collected in Table 1. The results are similar to those of linear polymers: for the most simple case (no HI, no EV, no FENE) the theoretical result $a=2$ is reproduced by our simulations, and for the more real models (HI, EV, FENE) exponents close to 3/2 are predicted.

The peculiarity of the ring topology in sheared chains can

Table 1
Exponents, a, of the power law for deformation δ^2

	No-HI	HI
IDEAL	2.01 ± 0.07	1.82 ± 0.07
THETA	1.82 ± 0.04	1.65 ± 0.02
GOOD	1.58 ± 0.04	1.52 ± 0.03

be analyzed looking at the values of δ^2 of ring and linear chains of the same length under comparable conditions. The effect of shear on polymer behavior is gauged by the β parameter, that combines the shear strength and the size of the chain. Fitting results for linear and ring chains to Eq. (10), with a common exponent $a\approx1.6$, we obtain $\delta_l^2/\delta_r^2 = C_l/C_r \approx 3.9$ for good solvent conditions, valid for a wide range of β in the intermediate region where Eq. (10) holds.

This ratio, for a common β, contains the effect of topology arising from the differences in $[\eta]$, which enters in the definition of β (Eq. (3)). With a more practical perspective, we can consider the ring-to-linear ratio achieved for polymers with the same molecular weight and in the same instrumental conditions, i.e. for the same shear rate $\dot{\gamma}$. In this case, the ratio is $\delta_l^2/\delta_r^2 = (C_l/C_r)q_{\eta,0}^{-a}$. With the ratio of intrinsic viscosities reported above, we obtain $\delta_l^2/\delta_r^2 \approx 9.1$, which indicates that the ring polymers are markedly less deformed than linear ones. Furthermore, as $\delta^2 \approx \langle s^2 \rangle/\langle s^2 \rangle_0$ for a sufficiently high shear rate, we have

$$q_s = q_{s,0} \frac{\delta_r^2}{\delta_l^2} \approx 0.059 \qquad (11)$$

Thus, while the square radius of gyration, $\langle s^2 \rangle$, of the ring polymer is about half of that its linear counterpart in a solution at rest, when the solution is sheared $\langle s^2 \rangle$ of the ring is about 16 times smaller than that of the linear chain. Again, it is clear that rings deform in strong shear much less than linear chains. Fig. 4(a) shows the shear rate evolution of the intrinsic viscosity (relative to its zero-shear value) of ring polymers of several N with HI and in good solvent conditions. As expected, β makes $[\eta]/[\eta]_0$ values N independent except at very high shear rates. The viscosity curve presents three clear different regions. Region I is the Newtonian plateau, characteristic at low shear rate ($\beta\leq1$ in our plots). Region III is the shear-thinning region, characteristic of most macromolecular fluids, where viscosity decreases strongly with shear rate. This non-linearity arises because molecules are highly oriented along the flow direction and close to fully stretched. The slope of this region in our log–log plot is about -1, which is indeed an upper limit characteristic of the FENE spring model. Experimental slopes are usually smaller (in absolute value) than -1.

However, it must be noticed that experiments usually do not reach such high shear rates and solutions are not infinitely dilute. Finally, an interesting part is region II, which could be termed as 'pseudo-plateau'. There, the viscosity diminishes slightly with β, before the clear shear-thinning region. This is a kind of behavior found when the Lennard-Jones potential, representing either theta or good solvent conditions, is present. Fig. 4(b) corresponds to the same kind of representation as Fig. 4(a) for a ring chain with $N=25$ both in the absence of intramolecular potential (ideal chain) and with intramolecular LJ potential representing both good and theta solvent conditions. As observed, the
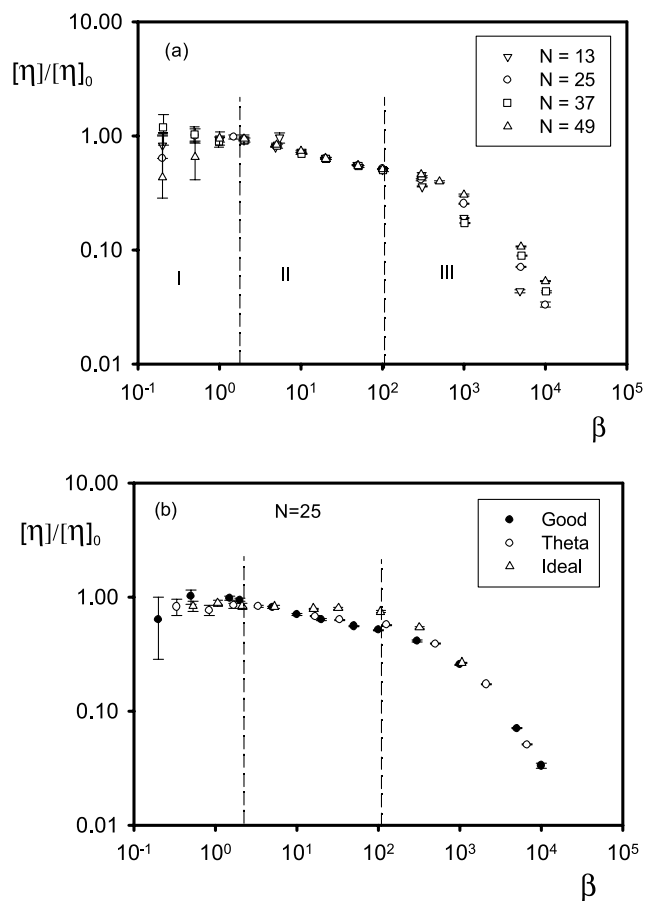
Fig. 4. (a) Intrinsic viscosity, $[\eta]/[\eta]_0$, vs. β of rings with several N, HI and good solvent conditions. (b) Intrinsic viscosity, $[\eta]/[\eta]_0$, vs. β of rings with $N=25$, HI and several solvent conditions.
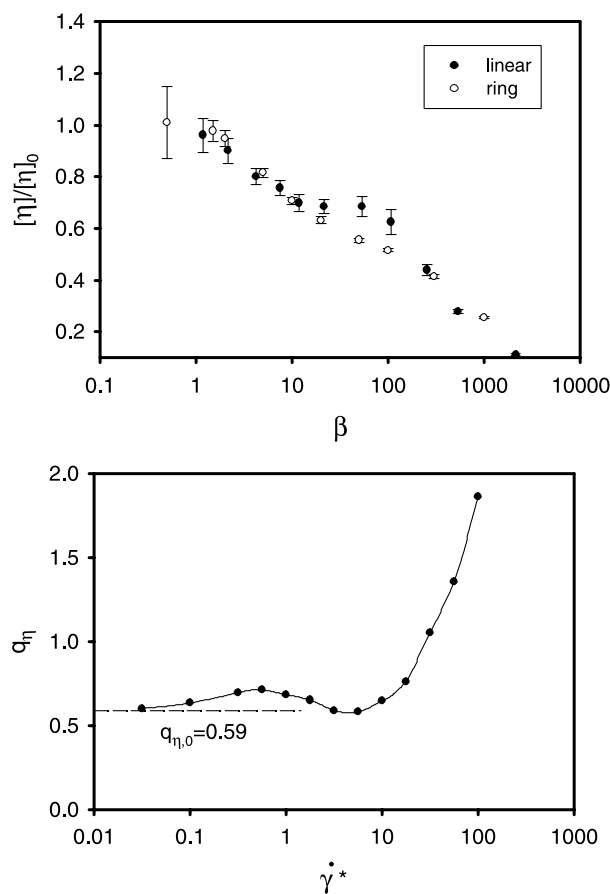

Fig. 5. (a) Semilog plot of the shear rate dependence of the intrinsic viscosity for both a linear and a ring chain with $N=25$, HI and good solvent conditions. (b) Semilog plot of the evolution of the ring-to-linear intrinsic viscosity ratio, q_η, with $\dot{\gamma}*$ for chains with $N=25$, HI and good solvent conditions.

solvent quality (good or theta) modeled with a LJ potential has no effect on the viscosity curve and points for both cases superimpose quite well, appearing the above commented pseudo-plateau (region II). However, the curve corresponding to an ideal chain (empty triangles) does not present the slowly decreasing region II and only two regimes, namely Newtonian plateau and shear thinning, are clearly distinguished. In any case, the onset of the shear-thinning region appears about the same value of β. The observation of the intermediate pseudo-plateau region for ring polymers follows a similar observation for linear polymers [25].

By carrying out simulations for ring and linear chains under comparable conditions, the effect of topology on non-Newtonian behavior can be ascertained. Fig. 5(a) shows the shear rate dependence of the intrinsic viscosity in the intermediate region, where $[\eta]$ falls to about one tenth of $[\eta]_0$, which is the one that could be accessible in experiments. The variation of $[\eta]$ in this region, as commented above, results from simultaneous effects of EV and HI and is similar but not coincident for the two topologies.

As we showed for δ^2, the comparison of the shear influences can be made directly in terms of the shear rate $\dot{\gamma}$.

Values of $[\eta]/[\eta]_0$ at a common $\dot{\gamma}$ can be combined to yield a shear-dependent ring-to-linear ratio of viscosities,

$$q_\eta = \frac{[\eta]_r}{[\eta]_l} \qquad (12)$$

Values of q_η as a function of shear rate are presented in Fig. 5(b). Note that if the non-Newtonian effect is represented by the ratio $[\eta]/[\eta]_0$ then we would have

$$q_\eta = \frac{[\eta]_r/[\eta]_{r,0}}{[\eta]_l/[\eta]_{l,0}} q_{\eta,0} \qquad (13)$$

In the intermediate region, q_η varies in a complex fashion, taking values higher than $q_{\eta,0}$ at high $\dot{\gamma}$. At a common $\dot{\gamma}$, the rings are 'less non-Newtonian' than their linear counterparts. Thus, in this intermediate region of moderate, likely accessible shear rates, the viscosity of ring chains approaches and even surpasses that of linear chains.

3.3. Elongational flow

When flexible polymers are subjected to an elongational rate of strain greater than a certain threshold value they

experience an abrupt increase in their conformation dependent properties due to the sudden unraveling of the random coil [2]. In this paper, we are concerned with the dependence of the average steady-state properties on the elongational rate. This kind of study allows for the determination of the critical elongational strain rate value, $\dot{\varepsilon}_c$.

Fig. 6(a) illustrates clearly the coil-stretch phenomenon for a ring chain of 25 beads with HI. There, the ratio of the elongational intrinsic viscosity, $[\bar{\eta}]$, to its equilibrium value $3[\eta]_0$, $[\eta]_0$ being the zero-shear intrinsic viscosity (Trouton relation), is represented vs. the elongational rate of strain. The elongational intrinsic viscosity is defined as

$$[\bar{\eta}] = \frac{N_A}{\eta_s M} \frac{\tau_{xx} - \tau_{yy}}{\dot{\varepsilon}} \tag{14}$$

where τ_{xx} and τ_{yy} are the normal components of the stress tensor, parallel and perpendicular to the flow, respectively. The polymer contribution to the components of the stress tensor is computed according to Eq. (9). As observed, at low $\dot{\varepsilon}$ the elongational viscosity is independent of the flow rate, as corresponds to the Newtonian regime. However, at $\dot{\varepsilon} \geq \dot{\varepsilon}_c$ the viscosity increases abruptly, giving the characteristic elongational-thickening behavior of polymer solutions. As explained in the previous section, at very high flow rates, the curve tends to reach a plateau when FENE springs reach their maximum elongation. A commonly used property to monitor experimentally the coil-stretch transition is the flow birefringence. In Fig. 6(b) the value of the dimensionless birefringence Δn^*, i.e. the birefringence Δn normalized to its limiting value for the fully-stretched chain, Δn_∞, is represented vs. the elongational rate. Thus, Δn^* tends to 1 as $\dot{\varepsilon}$ increases. The normalized birefringence is computed as

$$\Delta n^* = \frac{\Delta n}{\Delta n_\infty} = \frac{1}{(N-1)Q_{max}} \sum_{j=1}^{N-1} \langle (Q_j^x)^2 - (Q_j^y)^2 \rangle \tag{15}$$

where Q_j^α refers the α component of the connector vector j (i.e. the spring connecting beads j and $j+1$) and Q_{max} is, as defined before, the maximum spring length. As expected, at low $\dot{\varepsilon}$ the birefringence is independent of the flow rate and at $\dot{\varepsilon} \geq \dot{\varepsilon}_c$ its value increases suddenly. Analogously, Fig. 6(c) displays the results for the steady-sate values of the mean square radius of gyration, $\langle s^2 \rangle$, as a function of $\dot{\varepsilon}$ for ring chains of 25 beads with HI and in both theta and good solvent conditions. In addition, some results for Hookean, instead of FENE, springs have been included to illustrate the model independency of the critical value of the elongational rate. The coil-stretch transition is again clearly seen as a large, sudden increase in $\langle s^2 \rangle$ at a certain value of $\dot{\varepsilon}_c$. Thus at $\dot{\varepsilon} < \dot{\varepsilon}_c$, chains stay near their equilibrium coil conformations and therefore dimensions of the chain in a good solvent (black symbols) are slightly higher than in a theta solvent (empty symbols). However, the stretching process is so sharp that chains, irrespective of the model and solvent power considered, experience the transition around the same $\dot{\varepsilon}_c$. The value of the critical elongational rate is, instead, strongly dependent on the molecular weight of the polymer (number of beads in our bead-spring model) as well as the presence or absence of HI, as discussed in our previous paper [4], where the power law relating the critical rate to the polymer length for linear chains was determined. It is then the purpose of the last part of this paper to show the exponent arising for ring polymers both with and without HI.

The strong effect of the coil-stretch transition on polymer properties makes the value of $\dot{\varepsilon}_c$ easily computable. The case of Gaussian (Hookean) chains is particularly simple due to their infinite extensibility. Thus, in a computer experiment the radius of gyration of a single chain, initially in a coiled conformation, is monitored as the chain is stretched by an elongational flow of fixed $\dot{\varepsilon}$. As soon as $\dot{\varepsilon} \geq \dot{\varepsilon}_c$ the chain will
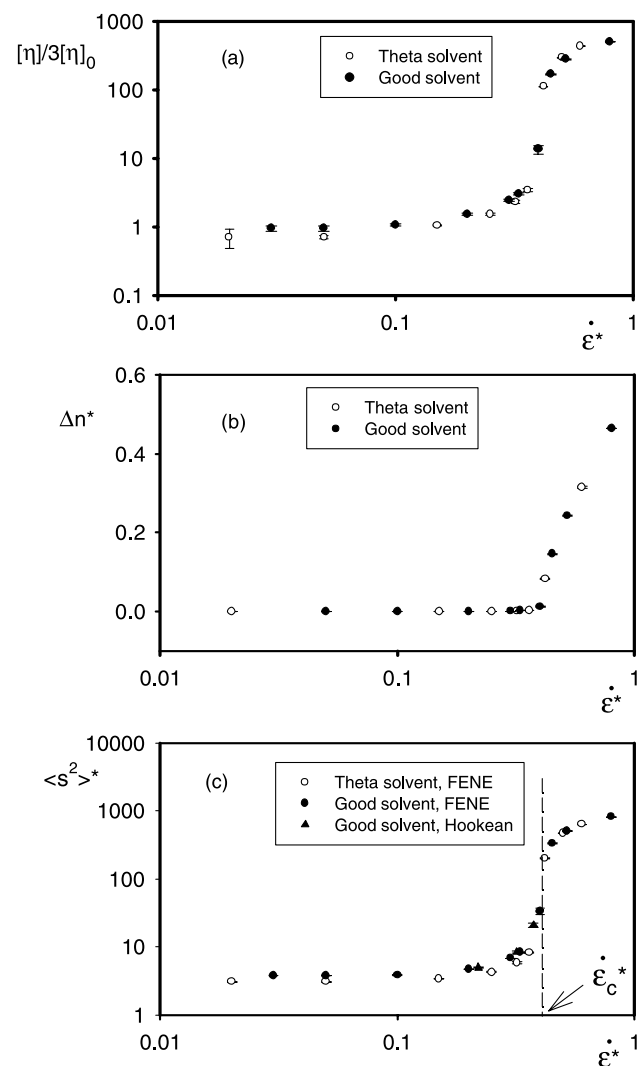
Fig. 6. (a) Evolution of the elongational intrinsic viscosity (normalized to its equilibrium value) with the dimensionless elongational rate, $\dot{\varepsilon}^*$ for a ring with $N=25$, HI and theta and good solvent conditions. (b) Evolution of the normalized birefringence with $\dot{\varepsilon}^*$ for a ring with $N=25$, HI and both theta and good solvent conditions. (c) Evolution of the dimensionless mean squared radius of gyration, $\langle s^2 \rangle^*$ with $\dot{\varepsilon}^*$, for a ring with $N=25$. Theta and good solvent and FENE and Hookean springs are considered.

rapidly and limitlessly grows in size. In this way, $\dot{\varepsilon}_c$ can be encompassed using a series of simulations with different $\dot{\varepsilon}$. In order to refine the determination of $\dot{\varepsilon}_c$, the single-molecule run is repeated a few times with different starting conformations. For FENE chains, a similar strategy is employed. However, as chain size is kept limited, another practical criterion must be imposed to check for coil-stretch transition. In this work, we consider that the transition takes place as soon as the radius of gyration reaches fifty times its equilibrium value, $s_{\text{trans}}^2 = 50 s_0^2$. The transition is so sharp, that several criteria can be used without influence on the critical value obtained. Following this procedure for rings with different N, the plots in Fig. 7 are drawn. This figure shows, in a log–log plot, the scaling relationships between $\dot{\varepsilon}_c$ and N for rings with and without HI and both good and theta solvent conditions. As shown, the slope is the same regardless of solvent power, but depends upon the inclusion or not of HI effects. In the absence of HI, we get the equality $\dot{\varepsilon}_c^* = (100 \pm 10) N^{(-2.00 \pm 0.05)}$, which agrees with the well-known quadratic power law governing free-draining (no-HI) linear chains. On other hand, in presence of HI (non-draining chains) we get $\dot{\varepsilon}_c^* = (51 \pm 3) N^{(-1.556 \pm 0.014)}$. Both scaling relationships are in perfect agreement with previous computational results obtained for linear chains [4]. Therefore the exponent of the foregoing power law is maintained when changing from a linear to a cyclic topology, varying just in the factor multiplying N. In conclusion, the power law found experimentally in theta solvents [2,26]

$$\dot{\varepsilon}_c = C_\varepsilon^r N^{-3/2} \tag{16}$$

is reproduced by simulations with non-preaveraged HI and holds for both ring and linear chains. By forcing our simulation results with HI to fit Eq. (16), i.e. the exponent of the power law to be exactly 3/2, we get a $C_\varepsilon^r \simeq 48.0$. From our previous work [4] we obtained for linear chains with HI a proportionality constant $C_\varepsilon^l \simeq 11.7$. Therefore the ratio of the critical elongational rate of ring chains, $\dot{\varepsilon}_c^r$, to that of linear chains, $\dot{\varepsilon}_c^l$, with the same length N or molecular weight, M, is a constant independent of chain length,

$$\frac{\dot{\varepsilon}_c^r}{\dot{\varepsilon}_c^l} = \frac{C_\varepsilon^r}{C_\varepsilon^l} \simeq 4.1 \tag{17}$$

The critical elongational rate of rings is about four times larger than that of linear chains. As we showed in the case of shear rate, rings are more resistant to flow deformation.

4. Summary

In this paper, we have used Brownian dynamics and the bead-spring model to study the flow behavior of cyclic polymers. Both in simple shear and uniaxial elongational flow, the ring chains present a qualitative behavior analogous to that of linear polymers. Under shear, the deformation of the chain scales with the dimensionless shear rate following a power law whose exponent value depends on the inclusion or not of intramolecular interactions. Under ideal conditions, without HI and EV interactions, the well-established quadratic power law, $\delta^2 = C\beta^2$, holds. Nevertheless the inclusion of excluded volume and hydrodynamic interaction tend to diminish the exponent value, thus the deformation becoming more difficult that under ideal conditions. This kind of behavior is also expected for linear polymers [24]. On other hand, the shear intrinsic viscosity is shown to present the classical behavior of polymer solutions: a Newtonian plateau at law shear rates and a power law decay at high shear rates, the so-called shear-thinning region. When excluded volume is present, the non-Newtonian regime starts with a soft decay in the viscosity before reaching the steep true shear-thinning region. Analogous to the usual data analysis at equilibrium, a comparison between linear and ring polymers was carried out through the ring-to-linear ratios of the radius of gyration and the intrinsic viscosity, e.g. q_s and q_η, evaluated at comparable shear rates. We found that $q_s \approx 0.059$, which indicates that rings deform under strong shear much less than their linear counterparts. On the other hand, the value of q_η depends on shear, behaving in a complex way at moderate shear rates and increasing at strong shear rates. In any case, $q_\eta \geq q_{\eta,0}$ which indicates that the viscosity of ring chains approaches and, at a high enough shear rate, even exceeds, that of linear chains.

Under elongational flow, cyclic polymers present the typical coil-stretch transition, analogous to that of linear chains. Indeed, the power law relating the critical elongational rate to the number of elements of the chain, N, i.e. its molecular weight, presents the same exponent for both linear and ring polymers, depending only on the presence or absence of HI. Clearly, to obtain results comparable with experiments, HI must be considered in the simulations. The proportionality constant of that scaling relationship is different for linear and ring polymers, the proportionality constant ratio, $C_\varepsilon^r / C_\varepsilon^l$, being about 4.
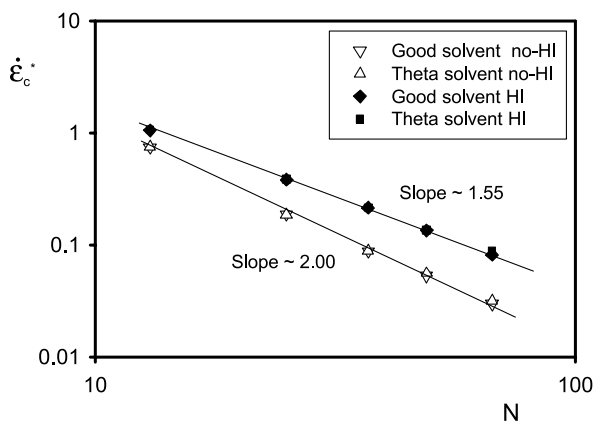

Fig. 7. Dependence of the dimensionless critical elongational rate, $\dot{\varepsilon}_c^*$, with ring size, N. All the possible interactions: no HI and HI, and theta and good solvent conditions are considered.

Acknowledgements

References

[1] De Gennes PG. J Chem Phys 1974;60:5030–42.

[2] Keller A, Odell JA. Colloid Polym Sci 1985;263:181–201.

[3] López Cascales JJ, Díaz FG, García de la Torre J. Polymer 1995;36: 345–51.

[4] Hernández Cifre JG, García de la Torre J. J Rheol 1999;43:339–58.

[5] Bensafi A, Maschke U, Benmouna M. Pol Int 2000;49:175–83.

[6] Yamakawa H. Modern theory of polymer solutions. New York: Harper & Row; 1971.

[7] Edwards CJ, Rigby D, Stepto RFT, Dodgson K, Semlyen JA. Polymer 1983;24:391–4.

[8] Edwards CJ, Rigby D, Stepto RFT, Semlyen JA. Polymer 1983;24: 395–9.

[9] Clarson SJ, Semlyen JA. Polymer 1986;27:1633–6.

[10] García Bernal JM, Tirado MM, Freire JJ, García de la Torre J. Macromolecules 1990;23:3357–62.

[11] García Bernal JM, Tirado MM, García de la Torre J, . Macromolecules 1991;24:593–8.

[12] Semlyen JA, editor. Cyclic polymers. 2nd ed. Dordrecht: Kluwer Academic; 2000.

[13] Bird RB, Curtiss CF, Armstrong RC, Hassager O., 2nd ed Dynamics of polymeric liquids, kinetic theory, vol. 2. New York: Wiley; 1987.

[14] Rey A, Freire JJ, García de la Torre J. Macromolecules 1987;20: 342–6.

[15] Freire JJ, Rey A, García de la Torre J. Macromolecules 1986;19: 457–62.

[16] Ermak DL, McCammon JA. J Chem Phys 1978;69:1352–60.

[17] Iniesta A, García de la Torre J. J Chem Phys 1990;92:2015–9.

[18] Rotne J, Prager S. J Chem Phys 1969;50:4831–7.

[19] Yamakawa H. J Chem Phys 1970;53:436–43.

[20] Öttinger HC. J Non-Newtonian Fluid Mech 1987;26:207–46.

[21] Mckenna GB, Hostetter BJ, Hadjichristidis N, Fetters LJ, Plazeck DJ. Macromolecules 1989;22:1834–52.

[22] López Cascales JJ, Navarro S, García de la Torre J. Macromolecules 1992;25:3574–80.

[23] Knudsen KD, Elgsaeter A, López Cascales JJ, García de la Torre J. Macromolecules 1993;26:3851–7.

[24] Knudsen KD, Elgsaeter A, García de la Torre J. Polymer 1996;37: 1317–22.

[25] Hernández Cifre JG. PhD Thesis, Fac. de Química, Univ. de Murcia; 2000.

[26] Cathey CA, Fuller GG. J Non-Newtonian Fluid Mech 1990;34:63–88.